Adaptable electro-optic detection of THz radiation using a laser-written bull's-eye antenna

Heydarian, Hesam; Xie, Xitong; Vishnuradhan, Aswin; Cui, Wei; Weck, Arnaud; Gamouras, Angela; Ménard, Jean-Michel

Publisher's version / Version de l'éditeur:

https://doi.org/10.1038/s41598-024-84625-4

Scientific Reports, 15, 1, 2025-01-04

scientific reports

Check for updates

OPEN

Adaptable electro-optic detection of THz radiation using a laser-written bull's-eye antenna

Hesam Heydarian[1]✉, Xitong Xie[2], Aswin Vishnuradhan[1], Wei Cui[1], Arnaud Weck[1,2], Angela Gamouras[1,3] & Jean-Michel Ménard[1,3]✉

We report a nonlinear terahertz (THz) detection device based on a metallic bull's-eye plasmonic antenna. The antenna, fabricated with femtosecond laser direct writing and deposited on a nonlinear gallium phosphide (GaP) crystal, focuses incoming THz waveforms within the sub-wavelength bull's eye region to locally enhance the THz field. Additionally, the plasmonic structure minimizes diffraction effects allowing a relatively long interaction length between the transmitted THz field and the co-propagating near-infrared gating pulse used in an electro-optic sampling configuration. We show an increased detection sensitivity over a large spectral range extending from 1.4 THz to 3.1 THz with a peak enhancement factor of 3.1 at 2.7 THz. We demonstrate that this plasmonic structure is especially effective in monitoring THz signals affected by beam wandering or varying spot sizes. Our concept can be adapted to any second-order nonlinear crystal to realize compact and sensitive THz detectors without the need for tight beam focusing or high-precision alignment. This work paves the way for future developments of compact and sensitive THz detectors, notably for applications in wireless communications.

Keywords Terahertz detector, Nonlinear optics, Plasmonic, Electro-optic sampling

Improving the sensitivity of terahertz (THz) detection techniques is fundamental to the deployment of THz-based systems to enable new applications in imaging and spectroscopy[1], ultrafast wireless communications[2], and security screening[3]. The most widely used techniques for the detection of THz pulses in the range of 0.5–30 THz are based on nonlinear optical processes[4]. In particular, THz detection techniques relying on nonlinear optical effects, such as electro-optic sampling (EOS), are powerful and versatile techniques which have the potential to reach high detection sensitivity over a broad operational spectral bandwidth[5,6]. The EOS technique exploits the $\chi^{(2)}$ nonlinearity of an electro-optic crystal and can be explained in the context of the Pockels' effect: the incoming THz pulse acts as an oscillating electric field changing the polarization state of a co-propagating femtosecond near-infrared (NIR) gating pulse through a second-order nonlinear effect. The THz wave amplitude and phase can then be fully mapped out by monitoring the polarization state of the gating pulse while the time delay is scanned between the two pulses. The sensitivity of this nonlinear detection technique depends on many factors such as the materials' $\chi^{(2)}$ coefficient, the interaction length and the phase matching conditions. Previous work reported on different optical geometries to increase detection sensitivity[7–9], notably by controlling phase matching conditions, but other parameters like the minimum size of the THz spot are often overlooked. Since a smaller spot size corresponds to a larger field amplitude, EOS setups usually rely on strong focusing optics. However, because of the diffraction limit, the THz spot size always remains large in comparison to gating beam diameter, which typically remains an order of magnitude smaller. Therefore, a configuration able to achieve sub-wavelength confinement of a THz wave within an electro-optic crystal can greatly enhance the sensitivity of the EOS technique. Such solutions have been explored previously in the context of electro optic phase shifters[10–12]. In this previous work, a metallic bowtie antenna locally enhances the THz field within a small μm-scale interaction region to achieve more efficient nonlinear interactions[10]. This field enhancement arises from the excitation of plasmon modes, coherent oscillation of the conduction electrons along the metal surface[13], and the confinement of the electromagnetic field near the metal surface, which leads to a more efficient nonlinear optical detection[14]. In a more recent design, an optimized spatial overlap was achieved by developing a monolithic detector on a silicon-photonics platform resulting in orders of magnitude improvement of the nonlinear conversion efficiency per unit length compared to bulk nonlinear crystals[11,12]. However, in this device,

[1]Department of Physics, University of Ottawa, Ottawa, ON K1N 6N5, Canada. [2]Department of Mechanical Engineering, University of Ottawa, Ottawa, ON K1N 6N5, Canada. [3]National Research Council Canada, Ottawa, ON K1A 0R6, Canada. ✉email: hheydari@uottawa.ca; jean-michel.menard@uottawa.ca

the guided plasmonic probe beam interacts with the enhanced THz field in a noncollinear manner, which drastically limits the interaction length. In addition, these configurations rely on nonlinear organic materials and are therefore more susceptible to optical damage than semiconductor-based devices. Plasmonic nanostructures have also been used in photoconductive antennas (PCA) to enhance the THz detection sensitivity by amplifying the optical absorption and photocarrier generation in an active region[15,16]. In other designs using plasmonic contact electrodes[17] and plasmonic antenna arrays[18], further enhancements in detection sensitivity over a large spectral bandwidth are achievable due to the smaller path length of photo-generated carriers to the electrodes. Despite these advancements, the performance of PCA detectors is still limited by a narrow operational bandwidth confined to relatively low THz frequencies and a relatively slow response time due to the slow drift velocity of the photo-generated carriers[18].

In this work, we present a plasmonic bull's-eye antenna designed to increase THz detection efficiency in a standard free-space EOS configuration. The antenna, fabricated with a laser direct machining method and positioned on the surface of a GaP crystal, captures the incoming THz field and focusses it within the sub-wavelength bull's eye region, where a NIR gating pulse is also focused. The resulting local field-enhancement of the THz wave leads to a stronger nonlinear interaction with the gating pulse and an improved detection efficiency. In addition, the antenna's design minimizes diffraction effects of the transmitted THz field as it overlaps with the NIR pulse propagating inside the GaP crystal. This extended spatial overlap results in a longer nonlinear interaction length, further enhancing THz detection sensitivity. We experimentally confirm a detection sensitivity enhancement across a wide spectral window, ranging from 1.4 to 3.1 THz, with a three-fold increase at the resonance frequency of 2.7 THz. Although we demonstrate the concept on GaP, a semiconductor crystal, any second-order nonlinear materials could be implemented in this EOS configuration to access different operational frequencies. Finally, our device demonstrates the capability to mitigate the impact of THz beam wandering and size fluctuations at the receiver position. Combined with detection schemes relying on an up-conversion process[5] or thermal-based nanomechanical resonators[19], the device could significantly improve the monitoring of wireless signals for future communication technologies exploiting >1 THz frequencies[20,21] and single pixel imaging[22,23].

Experiments and results

A schematic diagram of the antenna structure design is shown in Fig. 1a,b. This structure is composed of several concentric gold ridges of width (w) and grating period (p), referred to as a bull's-eye grating, to couple the normal incidence THz wave into a surface plasmon polaritons (SPP) propagating towards the central aperture. This gold layer is attached to a 110-oriented GaP substrate, a second-order nonlinear crystal. The ridges' size and grating period are engineered to maximize the local THz field enhancement at the center of the structure and to optimize the directionality of its near-field reemission pattern in the nonlinear substrate. When a femtosecond near-infrared (NIR) gating pulse is transmitted in the central aperture, nonlinear interactions between this beam and the enhanced THz field produce the signal recorded by the electro-optic sampling scheme. The signal

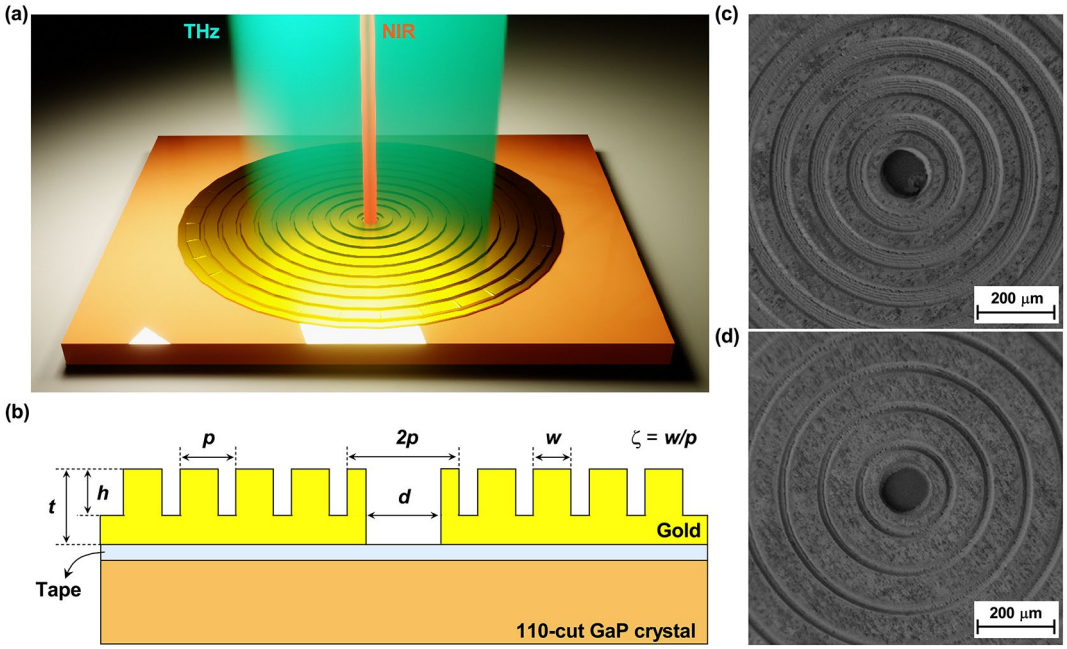

Fig. 1. Nonlinear THz plasmonic detection device. (**a**) Schematic of the bull's-eye plasmonic antenna on a GaP crystal with an incident THz wave (cyan). An incident NIR gating beam (red) overlaps with the enhanced THz field in the center of the structure (GaP inside), to increase EOS detection sensitivity. (**b**) Cross-sectional view of the bull's-eye detection device. (**c**,**d**) Show SEM images of devices A and B, respectively, which are fabricated with laser direct writing.

amplitude is proportional to the nonlinear interaction strength, which depends on both the THz field and the spatiotemporal overlap of the two beams inside the nonlinear material. Temporal overlap is easily achieved by controlling the delay of the gating pulse with a translation stage in a standard EOS set-up, while an optimized spatial overlap requires thoughtful design of the plasmonic antenna. Numerous designs have been used to achieve a substantial local field enhancement. Yet, such high fields are typically confined near the plasmonic structure and do not take advantage of a long nonlinear interaction length. Therefore, we designed a plasmonic structure that not only amplifies the THz field but also ensures its extension within the nonlinear crystal. This extension is crucial to allow for a relatively long co-propagation distance with the gating pulse, thereby maximizing the advantages of the structure.

Numerical simulations using the Lumerical FDTD software are used to optimize the antenna design. Specifically, we used the THz mode volume enhancement (MVE) at a THz frequency Ω as a figure of merit indicative of the performance of a bull's-eye plasmonic structure in improving THz wave detection with EOS. The effective THz field contributing to the nonlinear process is considered to be the product of the THz field amplitude and a normalized gaussian function with lateral size equal to the measured NIR gating beam diameter (2σ). The MVE is defined as the ratio of the effective THz field amplitude, with (E_p) and without (E_0) the presence of the plasmonic antenna, integrated within a volume V. The volume is related by the propagation path of the NIR gating pulse inside the nonlinear crystal and limited to the thickness of the crystal.

$$MVE(\Omega) = \frac{|\int |E_p(\Omega)|exp(-\frac{r^2}{\sigma^2})dV|^2}{|\int |E_0(\Omega)|exp(-\frac{r^2}{\sigma^2})dV|^2} \tag{1}$$

We calculate the optimal geometrical parameters of the plasmonic antenna with numerical simulations by maximizing the MVE. In these simulations, we consider the complex-valued dielectric function of gold[24] and linear optical properties of GaP[25]. Two promising designs of bull's-eye plasmonic structures are obtained. Device A has a grating duty cycle $\zeta = 50\%$, corresponding to the ratio of the ridge's width w to the period of the grating p, while ζ is set to 75% for device B. Both designs use an aperture diameter $d = 125$ μm, which is a tradeoff to achieve tight THz field confinement while ensuring a wide-enough clear path for the NIR gating pulse used for EOS. The eye antenna grating is composed of ten gold rings, which are optimized in pitch size, $p = 100$ μm, and grating height, $h = 12$ μm, to maximize the MVE at 2.7 THz. The grating period can be adjusted to shift the device's optimal frequency of operation, as shown in the Supplementary Information. We selected 2.7 THz because it corresponds to a region where most electro-optic detection schemes, highly performant around 1 THz, exhibit a rapid decrease in sensitivity.

A 25 μm-thick gold foil is used to fabricate the antenna. A laser direct writing (LDW) method allows the grating structure to be etched on the gold foil surface in a maskless fabrication process. This method effectively tackles the practical challenges associated with fabricating thick metallic structures[26]. Unlike standard thin film coating techniques, such as e-beam and thermal evaporation, which are limited to coating thicknesses of only a few hundred nanometers, this approach allows for greater flexibility and scalable fabrication of thick structures adapted for THz applications. The LDW system is equipped with a Yb:KGW laser source delivering 300 fs pulses at a wavelength of 1030 nm and repetition rate of 10 kHz. Using a 10 mW focused Gaussian beam with a diameter of 8 μm on the gold surface, we achieve vertical and lateral resolution as small as 8 μm and 1.5 μm, respectively. The relatively low laser power increases control over the vertical etch rate while reducing thermal accumulation. The beam scanning speed of 1 mm/s ensures no deformation in the circular shape of the eye antenna rings. With these parameters, a groove with 50 μm width and 12 μm depth is fabricated by scanning the laser beam 8 times, then the beam is moved laterally by 7 μm, and the process is repeated seven times to cover the full device width. Figure 1c,d show the SEM image of the fabricated structures.

We evaluate the improved performance of an EOS detection scheme with our plasmonic device located on the surface of a GaP nonlinear detection crystal. The experiment uses a standard home-built ultrafast time-domain THz spectrometer (THz-TDS)[27]. This scheme relies on a 5 W femtosecond fiber laser source (Vinci from TeraXion) producing 55 fs pulses with a repetition rate of 40 MHz at a wavelength of 1064 nm. The output is split into two beam paths for THz generation and detection. THz generation is achieved by optical rectification by focusing the NIR pulse on a 1 mm-thick 110-orientated GaP crystal. Within an enclosure purged with dry air, the generated THz wave is focused onto a reference THz detection crystal, a 200 μm-thick 110-oriented GaP. The minimum diameter of the focused THz beam is 125 μm at full width at half maximum (FWHM). The measurement setup is optimized in such a way that by translating the detection crystal along the optical propagation axis, the THz spot size on detection crystal increases up to 340 μm while the gating beam spot size is kept constant by adjusting the position of a focusing mirror. Exploring different THz spot sizes ranging up to several hundreds of microns is useful to assess the performance of a detector without the requirement of a tight focusing configuration. A quarter-wave plate, Wollaston prism and a pair of balanced photodiodes monitor the THz-induced polarization change as a function of the time delay to map out the THz transient.

Figure 2a shows the EOS trace collected with devices A and B with a 340 μm FWHM THz spot size, which is compared to the results obtained with the reference crystal (black line in Fig. 2). Here, all GaP detection crystals are from the same original wafer, thus having the same thickness. The Fourier transform is applied to the time traces to retrieve the power spectrum and is shown in Fig. 2b.

The enhancement in detection sensitivity, attributable to the plasmonic structure, is distinctively evident in the frequency domain data. We extract the detection enhancement (DE) factor by calculating the ratio between the spectral power measured with and without the plasmonic structure and compare this value with the MVE numerically calculated with Eq. (1) using the design parameters of devices A and B. We observe a good overall agreement between the measured DE and the calculated MVE. These two devices are similar in

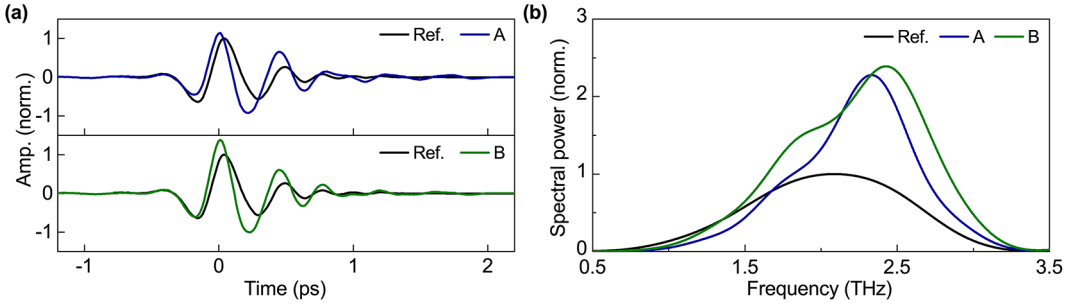

Fig. 2. THz measurement results. (**a**) THz transients measured by EOS with plasmonic structures A (blue line) and B (green line) or with the reference crystal (black line). (**b**) Corresponding spectral power obtained by Fourier transformation of the time-domain data.

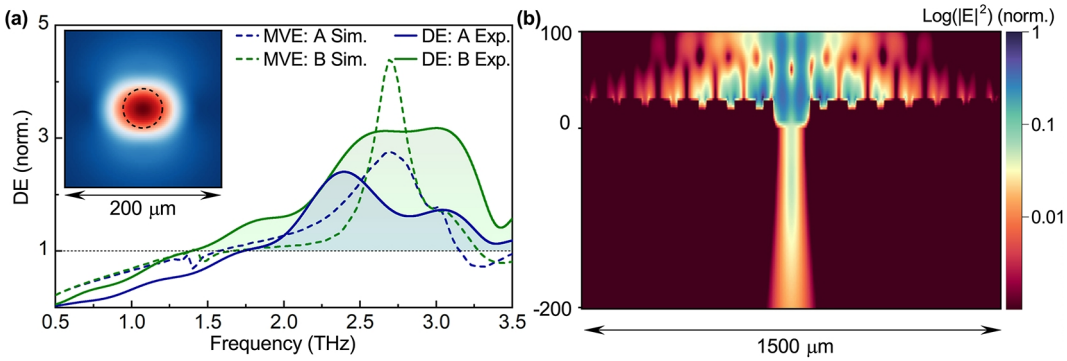

Fig. 3. Eye antenna performance as a THz detection device and THz field spatial distribution. (**a**) Experimental detection enhancement (DE) and calculated MVE for designs A (blue) and B (green). The inset shows the THz field distribution on the top surface of the GaP substrate under the antenna aperture of device B. The black dotted circles represent the NIR gating beam spot size (FWHM). (**b**) Normalized THz field intensity cross-section distribution at resonance frequency in the center of device B.

terms of enhancement around the resonance frequency, especially considering that defects induced during the fabrication process may broaden the spectral resonance. As shown in Fig. 3a, we reach experimental detection enhancement factors as high as 2.4 and 3.1 around the resonance frequency with devices A and B, respectively. Both experimental and numerical results confirm a higher detection efficiency with design B. Numerical simulations showing the spatial THz intensity distribution (Fig. 3b) indicate that the enhanced performance is attributed to the larger duty cycle. Also, as shown in Fig. S1a, the optimal device's performance is reached when the duty cycle is roughly 80%, similar to the specifications of device B ($\zeta = 75\%$). The THz electric field profiles also provide insights into the physical mechanism behind the enhancement of the nonlinear interaction strength with the gating pulse. First, we observe that the THz field distribution at the resonance frequency directly behind the eye antenna aperture has a Gaussian profile with FWHM of 60 μm (see inset of Fig. 3a). This spatial profile, only slightly larger than the intensity distribution of the gating pulse (50 μm FWHM), ensures an efficient nonlinear interaction. More importantly, the re-radiated THz field on the transmission side of the antenna, shown in Fig. 3b, remains well collimated and directional to ensure a relatively long co-propagation length with the gating pulse. Considering that the plasmonic device increases the detection sensitivity around the resonance frequency, a post processing step is needed to retrieve the spectrum of the incoming THz signal, which might be important for spectroscopy applications. This step consists in dividing the detected spectrum by the detection enhancement spectrum (shown in Fig. 3a). Such a step is, however, not necessary for most imaging and communication applications.

We explore the effect of different THz spot sizes impinging on the device while other parameters are kept constant. Here the THz spot size at focus is measured at the resonance frequency of the plasmonic structures, and the Gaussian beam theory is used to evaluate the beam size at different distances from the focal plane. Previous measurements shown in Figs. 2 and 3 are obtained at the detector position corresponding to the largest spot size (340 μm) tested in our experiments, which also resulted in the most significant detection enhancement. Figure 4a shows the measured DE at the resonance frequency, which remains larger than unity at all times but increases linearly with the THz beam diameter. The reason for this effect is due to a larger coupling of the THz wave to the grating surface, which partially compensates for the fact that the THz field is weaker. The MVE, also calculated at the resonance frequency, follows the same trend as the experimental measurements but indicates that a larger detection enhancement factor could be achieved, potentially by refining fabrication techniques to

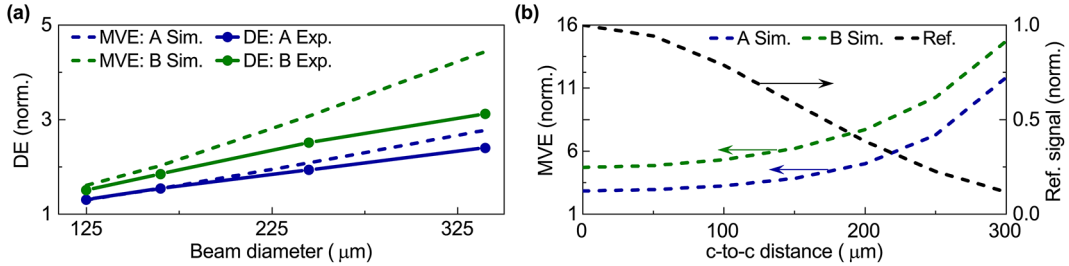

Fig. 4. Effect of tight beam focusing and misalignment on the device performance. (**a**) Experimental detection enhancement (DE) and calculated mode volume enhancement (MVE) of devices A and B as a function of the THz beam diameter (FWHM). (**b**) Calculated MVE of devices A and B, and normalized reference signal corresponding to numerically calculated overlap between the THz and gating beam without plasmonic devices as a function of center-to-center distance of THz and NIR gating beams.

decrease device imperfections. The deviation from the linear trend of the experimental results observed with the larger beam diameter is caused by scattering loss of the surface waves, which increases with propagation distance in larger THz beams. In Fig. 4b the effect of the misalignment and non-perfect spatial overlap between THz and gating pulse is demonstrated. As can be seen by changing the center-to-center (c to c) distance of the THz and NIR gating beams, the MVE increases while the reference signal decreases. As a result, the eye antenna structure can be used to partially compensate for beam steering effects and other sources of optical misalignment.

Conclusions

In summary, we investigate the effect of a custom designed bull's-eye plasmonic antenna on the surface of a nonlinear crystal in an EOS detection scheme. Numerical studies show that an incident THz wave excites a surface plasmon resonance and creates a local enhanced field in the central aperture with a field distribution extending within the nonlinear substrate. This antenna design ensures spatial overlap of the coupled THz field with a co-propagating near-infrared (NIR) gating pulse for efficient nonlinear interactions. Two plasmonic resonator designs were fabricated with a laser direct writing technique and tested experimentally with a time-resolved THz spectrometer. We observe a significant enhancement of THz detection at the resonance frequency, which can reach a factor of 3.1 when the incident THz spot size has a 340 μm diameter (FWHM). The concept of a bull's-eye plasmonic antenna could lead to major implications for the enhanced detection of free-propagating THz signals of a specific frequency. Given recent advancements in wireless communication at frequencies approaching 1 THz[20], our device could play a crucial role in enhancing detection sensitivity while mitigating the adverse effects of beam wandering, size fluctuations, and spatial distortion caused by environmental fluctuations.

Data availibility

Data underlying the results presented in this paper are not publicly available at this time but may be obtained from the corresponding author upon reasonable request.

Received: 1 October 2024; Accepted: 25 December 2024
Published online: 04 January 2025

References

1. Jepsen, P. U., Cooke, D. G. & Koch, M. Terahertz spectroscopy and imaging-modern techniques and applications. *Laser Photon. Rev.* **5**(1), 124–166 (2011).
2. Akyildiz, I. F., Jornet, J. M. & Han, C. Terahertz band: Next frontier for wireless communications. *Phys. Commun.* **12**, 16–32 (2014).
3. Kemp, M.C., Taday, P.F., Cole, B.E., Cluff, J.A., Fitzgerald, A.J. & Tribe, W.R. Security applications of terahertz technology. In *Terahertz for Military and Security Applications*, vol. 5070 (eds. Hwu, R.J., Woolard, D.L.) 44–52 (SPIE, 2003). https://doi.org/10.1117/12.500491. International Society for Optics and Photonics.
4. Lewis, R. A review of terahertz detectors. *J. Phys. D Appl. Phys.* **52**(43), 433001 (2019).
5. Jubgang Fandio, D. J. et al. Zeptojoule detection of terahertz pulses by parametric frequency upconversion. *Opt. Lett.* **49**(6), 1556–1559 (2024).
6. Cui, W. et al. Broadband and tunable time-resolved thz system using argon-filled hollow-core photonic crystal fiber. *APL Photon.* **3**(11) (2018).
7. Halpin, A. et al. Enhanced terahertz detection efficiency via grating-assisted noncollinear electro-optic sampling. *Phys. Rev. Appl.* **12**(3), 031003 (2019).
8. Cui, W., Awan, K. M., Huber, R., Dolgaleva, K. & Ménard, J.-M. Broadband and high-sensitivity time-resolved thz system using grating-assisted tilted-pulse-front phase matching. *Adv. Opt. Mater.* **10**(1), 2101136 (2022).
9. Porer, M., Ménard, J.-M. & Huber, R. Shot noise reduced terahertz detection via spectrally postfiltered electro-optic sampling. *Opt. Lett.* **39**(8), 2435–2438 (2014).
10. Benea-Chelmus, I.-C. et al. Three-dimensional phase modulator at telecom wavelength acting as a terahertz detector with an electro-optic bandwidth of 1.25 terahertz. *ACS Photon.* **5**(4), 1398–1403 (2018).
11. Salamin, Y. et al. Compact and ultra-efficient broadband plasmonic terahertz field detector. *Nat. Commun.* **10**(1), 5550 (2019).
12. Benea-Chelmus, I.-C. et al. Electro-optic interface for ultrasensitive intracavity electric field measurements at microwave and terahertz frequencies. *Optica* **7**(5), 498–505 (2020).
13. Kauranen, M. & Zayats, A. V. Nonlinear plasmonics. *Nat. Photon.* **6**(11), 737–748 (2012).
14. Koshelev, K. et al. Subwavelength dielectric resonators for nonlinear nanophotonics. *Science* **367**(6475), 288–292 (2020).

15. Jooshesh, A. et al. Plasmon-enhanced below bandgap photoconductive terahertz generation and detection. *Nano Lett.* **15**(12), 8306–8310 (2015).
16. Yardimci, N. T. & Jarrahi, M. Nanostructure-enhanced photoconductive terahertz emission and detection. *Small* **14**(44), 1802437 (2018).
17. Berry, C. W., Wang, N., Hashemi, M. R., Unlu, M. & Jarrahi, M. Significant performance enhancement in photoconductive terahertz optoelectronics by incorporating plasmonic contact electrodes. *Nat. Commun.* **4**(1), 1622 (2013).
18. Yardimci, N. T. & Jarrahi, M. High sensitivity terahertz detection through large-area plasmonic nano-antenna arrays. *Sci. Rep.* **7**(1), 42667 (2017).
19. Zhang, C. et al. High detectivity terahertz radiation sensing using frequency-noise-optimized nanomechanical resonators. *APL Photon.* **9**(12), 126105 (2024).
20. Shafie, A. et al. Terahertz communications for 6g and beyond wireless networks: Challenges, key advancements, and opportunities. *IEEE Netw.* **37**(3), 162–169 (2022).
21. Guerboukha, H., Zhao, B., Fang, Z., Knightly, E. & Mittleman, D. M. Curving thz wireless data links around obstacles. *Commun. Eng.* **3**(1), 58 (2024).
22. Zanotto, L. et al. Time-domain terahertz compressive imaging. *Opt. Express* **28**(3), 3795–3802 (2020).
23. Deng, Y., She, R., Liu, W., Lu, Y. & Li, G. High-efficiency terahertz single-pixel imaging based on a physics-enhanced network. *Opt. Express* **31**(6), 10273–10286 (2023).
24. Ordal, M. A., Bell, R. J., Alexander, R. W. Jr., Long, L. L. & Querry, M. R. Optical properties of au, ni, and pb at submillimeter wavelengths. *Appl. Opt.* **26**(4), 744–752 (1987).
25. Parsons, D. & Coleman, P. Far infrared optical constants of gallium phosphide. *Appl. Opt.* **10**(7), 1683–11685 (1971).
26. Benea-Chelmus, I.-C., Bonzon, C. & Faist, J. High-sensitivity intensity correlation measurements for photon statistics at terahertz frequencies. In *Terahertz, RF, Millimeter, and Submillimeter-Wave Technology and Applications X*, vol. 10103, 2–8 (SPIE, 2017).
27. Couture, N. et al. Compact, low-cost, and broadband terahertz time-domain spectrometer. *Appl. Opt.* **62**(15), 4097–4101 (2023).

Acknowledgements
Eeswar Kumar Yalavarthi, Nicolas Couture, and Ali Maleki for technical assistance and insightful discussions.

Author contributions
H.H., J.-M.M., and A.G. conceived the idea. H.H. performed the simulations. H.H. and X.X. conducted the device fabrication. H.H., A.V., and W.C. performed the test and measurement. J.-M.M., A.G., and A.W. supervised the project. H.H., J.-M.M., and A.G. wrote the original draft. All authors reviewed the manuscript.

Funding
This work was supported by Natural Sciences and Engineering Research Council of Canada (RGPIN-2023-05365); the High Throughput and Secure Networks Challenge Program at the National Research Council of Canada (HTSN 702, HTSN 254), and the Joint Centre for Extreme Photonics.

Declarations

Competing interests
The authors declare no competing interests.

Additional information
Supplementary Information The online version contains supplementary material available at https://doi.org/10.1038/s41598-024-84625-4.

Correspondence and requests for materials should be addressed to H.H. or J.-M.M.